Electronic Supplementary Material (ESI) for Journal of Materials Chemistry A.

—Supplementary Information— Synthetic control of structure and conduction properties in Na-Y-Zr-Cl solid electrolytes

Elias Sebti[1,2], Ji Qi[3], Peter M. Richardson[1], Phillip Ridley[3], Erik A. Wu[3], Swastika Banerjee[3,4], Raynald Giovine[1,2], Ashley Cronk[3], So-Yeon Ham[3], Ying Shirley Meng*[3,5], Shyue Ping Ong*[3], and Raphaële J. Clément*[1,2]

[1] *Materials Department, University of California, Santa Barbara, California 93106, United States*
[2] *Materials Research Laboratory, University of California, Santa Barbara, California 93106, United States*
[3] *Department of NanoEngineering, University of California San Diego, 9500 Gilman Dr., La Jolla, San Diego, California 92093, United States*
[4] *Present address: Department of Chemistry, Indian Institute of Technology Roorkee, Roorkee 247667, India*
[5] *Pritzker School of Molecular Engineering, University of Chicago, Chicago, IL, USA*

Contents

Sec. S1 **XRD Patterns Obtained on Na_2ZrCl_6 Samples** **S4**

Sec. S2 **Le Bail Refinement of Slow Cooled and Twice Ball Milled Na_2ZrCl_6 XRD Patterns** **S5**

Sec. S3 **Simultated ^{23}Na NMR Spectrum of Na_2ZrCl_6** **S6**

Sec. S4 **^{23}Na EXSY on Twice Ball Milled Na_2ZrCl_6** **S7**

Sec. S5 **Stacking faults in P$\bar{3}$m1 NZC** **S8**

Sec. S6 **Fits of the ^{23}Na VT-NMR Data Acquired on Twice Ball Milled Na_2ZrCl_6** **S10**

Sec. S7 **^{23}Na VT-NMR on Quenched Na_2ZrCl_6** **S12**

Sec. S8 **XRD Patterns Obtained on Na_3YCl_6 Samples** **S13**

Sec. S9 **SEM of Na_3YCl_6** **S14**

Sec. S10 **Simultated ^{23}Na NMR Spectrum of Na_3YCl_6** **S15**

Sec. S11 **^{23}Na EXSY on Twice Ball Milled Na_3YCl_6** **S16**

Sec. S12 **^{23}Na VT-NMR on Quenched Na_3YCl_6** **S17**

Sec. S13 **Microstructure Evolution of Quenched Na_3YCl_6 upon a 134 °C Heat Treatment** **S18**

Sec. S14 **Bond Valence Sum Maps of Na_2ZrCl_6 and Na_3YCl_6 Polymorphs** **S19**

Sec. S15 **Le Bail Refinement of Slow Cooled $Na_{2.25}Y_{0.25}Zr_{0.75}Cl_6$ XRD Pattern** **S20**

Sec. S16 **Raman of $Na_{2.25}Y_{0.25}Zr_{0.75}Cl_6$** **S21**

Sec. S17 **Energetics of Enumerated $Na_{2.25}Y_{0.25}Zr_{0.75}Cl_6$ Supercells** **S22**

Sec. S18 **^{23}Na EXSY of twice ball milled $Na_{2.25}Y_{0.25}Zr_{0.75}Cl_6$** **S23**

Sec. S19 **Cross-sectional SEM of $Na_{2.25}Y_{0.25}Zr_{0.75}Cl_6$ Pellets** **S24**

Sec. S20 **Improvement of Reliability of MTP with Active Learning** **S25**

Sec. S21 Simulated Evolution of Na Octahedral Site Occupancies in $Na_{2.25}Y_{0.25}Zr_{0.75}Cl_6$ S26

Sec. S22 Simulated Na Motion at 500 K in $Na_{2.25}Y_{0.25}Zr_{0.75}Cl_6$ S27

Sec. S23 Simulated Cl Motion at 400 K in $Na_{2.25}Y_{0.25}Zr_{0.75}Cl_6$ S28

Sec. S24 Evolution of Twice Ball Milled $Na_{2.25}Y_{0.25}Zr_{0.75}Cl_6$ EIS-derived Conductivity S29

Sec. S25 Metastability of the Twice Ball Milled $Na_{2.25}Y_{0.25}Zr_{0.75}Cl_6$ Structure S30

Sec. S26 Building NYC, NZC, and NYZC structural models for NMR CASTEP calculations S31

- Sec. S26.1 NZC S31
- Sec. S26.2 NYC S31
- Sec. S26.3 NYZC S31

Sec. S27 Parameter Convergence for NMR CASTEP Calculations S32

Sec. S28 ^{23}Na Chemical Shift Calibration Curve for Analysis of NMR CASTEP Calculation Results S33

Sec. S1 XRD Patterns Obtained on Na_2ZrCl_6 Samples

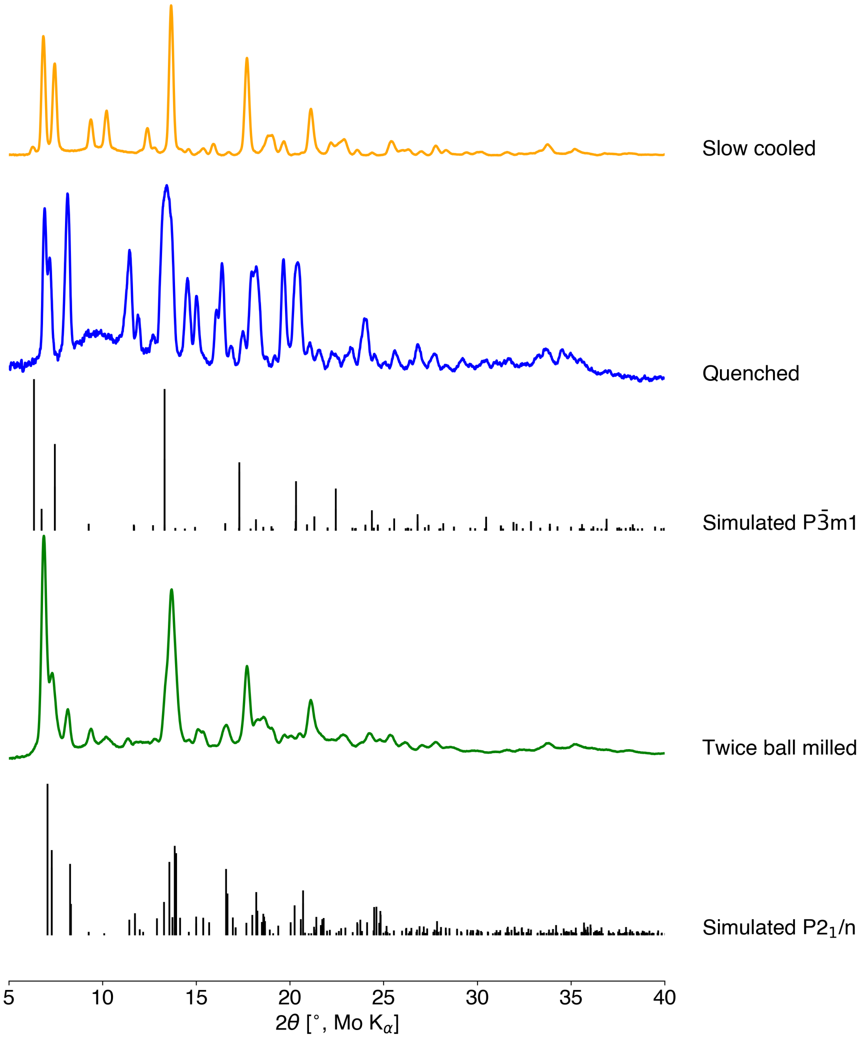

Figure S1: Comparison of simulated XRD patterns for lowest energy P$\bar{3}$m1 and P2_1/n Na_2ZrCl_6 enumerated model structures obtained from DFT and patterns obtained on the slow cooled, quenched, and twice ball milled samples. Quenched and twice ball milled patterns are reproduced from[1].

Sec. S2 Le Bail Refinement of Slow Cooled and Twice Ball Milled Na_2ZrCl_6 XRD Patterns

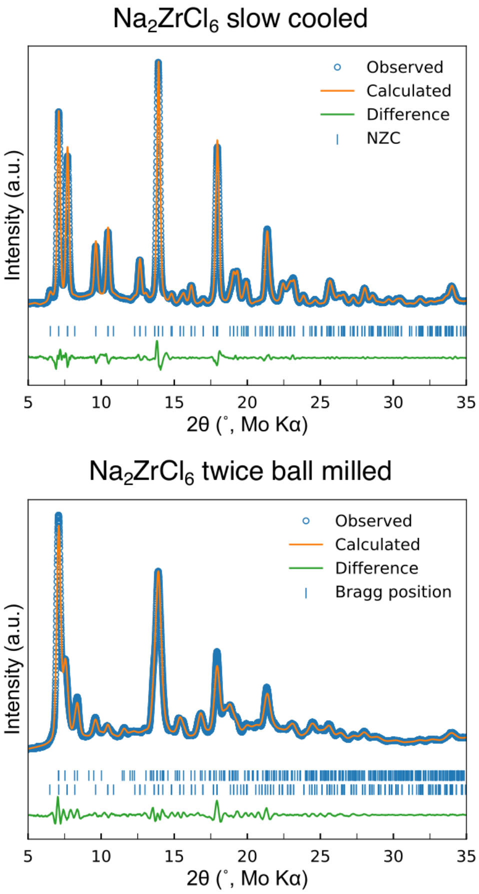

Na_2ZrCl_6 slow cooled

$P\bar{3}m1$
$a = b = 11.4767$ Å,
$c = 6.2464$ Å
$V = 712.5159$ Å^3

Na_2ZrCl_6 twice ball milled

Major phase: $P\bar{3}m1$
$a = b = 11.4609$ Å,
$c = 6.2661$ Å
$V = 712.7927$ Å^3

Minor phase: $P2_1/n$
$a = 6.7074$ Å, $b = 7.0561$ Å,
$c = 10.0243$ Å
$\alpha = \gamma = 90.000°$, $\beta = 93.4127°$
$V = 473.5934$ Å^3

Figure S2: Le Bail refinement conducted on the XRD patterns of slow cooled (top) and twice ball milled (bottom) Na_2ZrCl_6 samples. The twice ball milled pattern is reproduced from[1].

Sec. S3 Simultated ^{23}Na NMR Spectrum of Na_2ZrCl_6

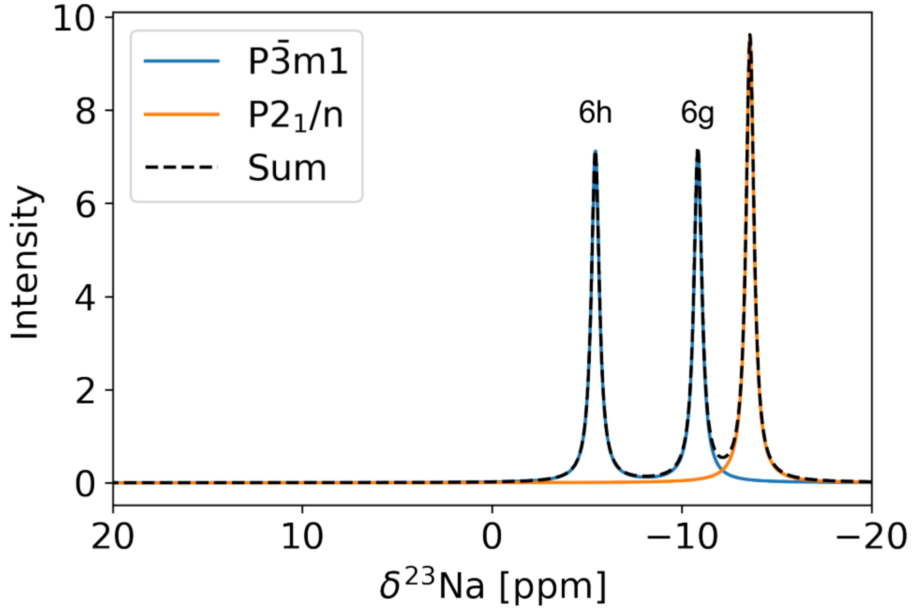

Figure S3: Reconstruction of the ^{23}Na NMR resonances expected for the Na_2ZrCl_6 P$\bar{3}$m1 and P2_1/n polymorphs using Lorentzian lineshapes centered at the calibrated chemical shift values obtained from NMR CASTEP simulations. For each computed shift, a signal linewidth of 0.5 ppm was used to best replicate experimentally-observed lineshapes across preparation methods.

Sec. S4 ^{23}Na EXSY on Twice Ball Milled Na_2ZrCl_6

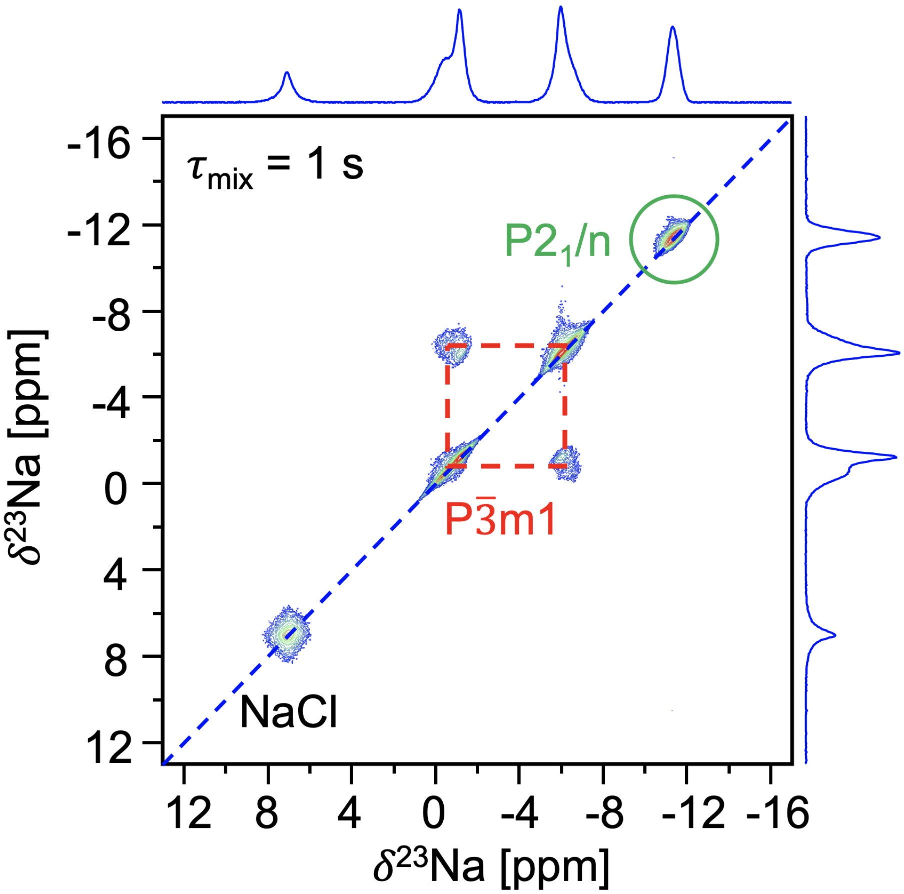

Figure S4: ^{23}Na 2D EXSY spectrum obtained on twice ball milled Na_2ZrCl_6 at 55 °C (328 K) and using a 1 s mixing time (τ_{mix}). The 1D spectrum collected on this sample is projected on the right hand side and at the top of the 2D spectrum. All spectra were acquired at 18.8 T using a 3.2 mm HX probe at a 10 kHz MAS spinning speed. Longitudinal relaxation times (T_1) for the two phases of Na_2ZrCl_6 were around 4 s, allowing minimal signal loss during the 1 s of mixing time.

Sec. S5 Stacking faults in P$\bar{3}$m1 NZC

While the ^{23}Na ss-NMR data collected on the quenched NZC sample (Figure 2 in the main text) indicates that the 6*g* and 6*h* Na sites of the P$\bar{3}$m1 phase are occupied in a 1:1 ratio, the Rietveld refinement of the synchrotron x-ray diffraction (sXRD) data on the same sample, presented in our earlier work[1], suggests that this ratio is closer to 3:1 ($F_{Na1(6g)}$= 0.73, $F_{Na2(6h)}$= 0.27). This discrepancy highlights the inability of Rietveld refinements to accurately determine the structure of quenched NZC, which we attribute to the presence of stacking faults, as explained below.

First, the error in the Na 6h and 6g site occupancies determined from Rietveld refinements of the sXRD data collected on quenched NZC was assessed by comparing the goodness of fit for two possible models of the P$\bar{3}$m1 phase. The sXRD data and its Rietveld refinement reproduced from Wu *et al.*[1] are shown in Figure S5. This structural model has a 3:1 occupation ratio of the 6*g* and 6*h* Na sites and fits the (001) reflection well but overestimates the intensities of the (10$\bar{1}$)and (21$\bar{1}$) reflections. The second structural model tested here, shown in Figure S5b, features the 1:1 6*g* to 6*h* occupation ratio based on our NMR results from Figure 2 of the manuscript, with the rest of the fitting parameters kept the same as in the first model. This second model overestimates the intensity of the (001) reflection but more appropriately fits the (10$\bar{1}$) and (21$\bar{1}$) reflections. Those two models have very similar r_{wp} parameters of 11.04 and 12.08, indicating that significant changes in the Na site occupancy ratio do not drastically affect the goodness of fit. Interestingly, while both models accurately fit most of the reflections, the (21$\bar{1}$) reflection observed experimentally is much broader than those predicted by the two models. Broadening of select reflections in the sXRD pattern is reminiscent of our prior work on the isostructural Li_3YCl_6 solid electrolyte, which contains a high concentration of stacking faults when prepared by high energy ball milling[2]. Other halide-based solid electrolytes have also been reported to contain stacking faults[3,4] and also exhibit selective broadening of XRD reflections. Hence, we believe that stacking faults in P$\bar{3}$m1 NZC are responsible for selective broadening of the (21$\bar{1}$) reflection. The (21$\bar{1}$) plane intersects the [0,0,0] Zr 1*a* site and this position is likely affected by stacking faults (see structural model in Figure S5c). Yet, a full analysis of the nature and extent of these stacking faults would require the use of specialized software, e.g., FAULTS[5], which is outside the scope of the present work.

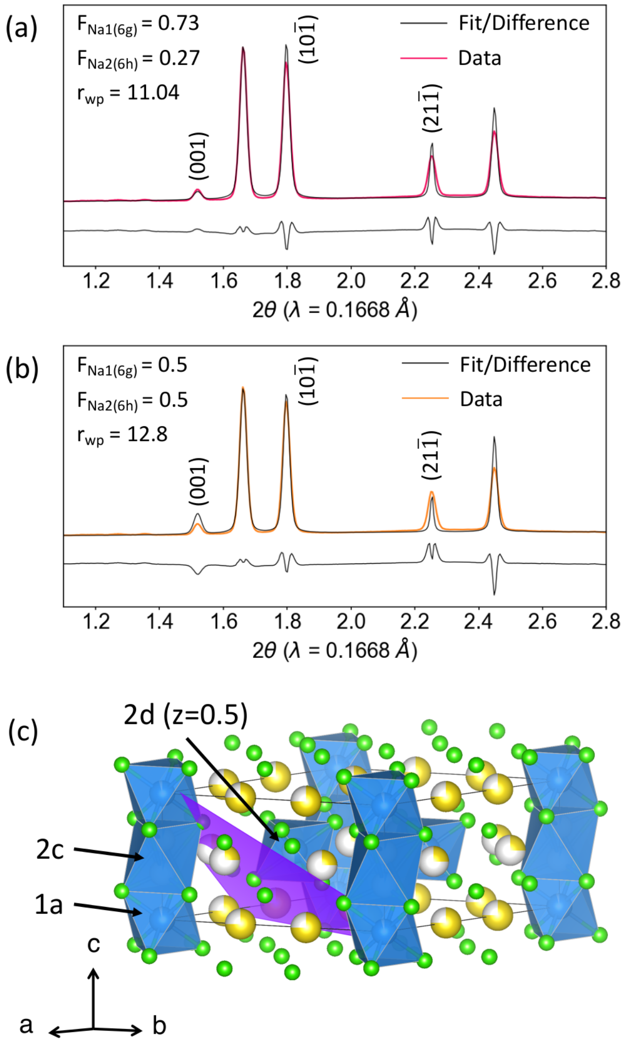

Figure S5: Rietveld refinements of the sXRD data collected on quenched NZC with the $6g$ and $6h$ sites of the P$\bar{3}$m1 phase occupied (a) in a ∼3:1 ratio, as previously reported[1], and (b) in a ∼1:1 ratio based on the site occupation ratio observed in the ^{23}Na ss-NMR spectrum shown in Figure 2 in the main text. The two models have very similar r$_{wp}$ parameters of 11.04 and 12.08, indicating that significant changes in the Na site occupancy ratio do not drastically affect the goodness of fit. Further, selective broadening of the (21$\bar{1}$) reflection suggests the presence of stacking faults in the P$\bar{3}$m1 NZC phase. (c) NZC P$\bar{3}$m1 crystal structure with the (21$\bar{1}$) plane shown in purple. Zr sites are labeled by their Wyckoff positions[1]. Color legend: Zr atoms are light blue, Cl atoms are light green, and Na atoms are yellow.

Sec. S6 Fits of the ^{23}Na VT-NMR Data Acquired on Twice Ball Milled Na_2ZrCl_6

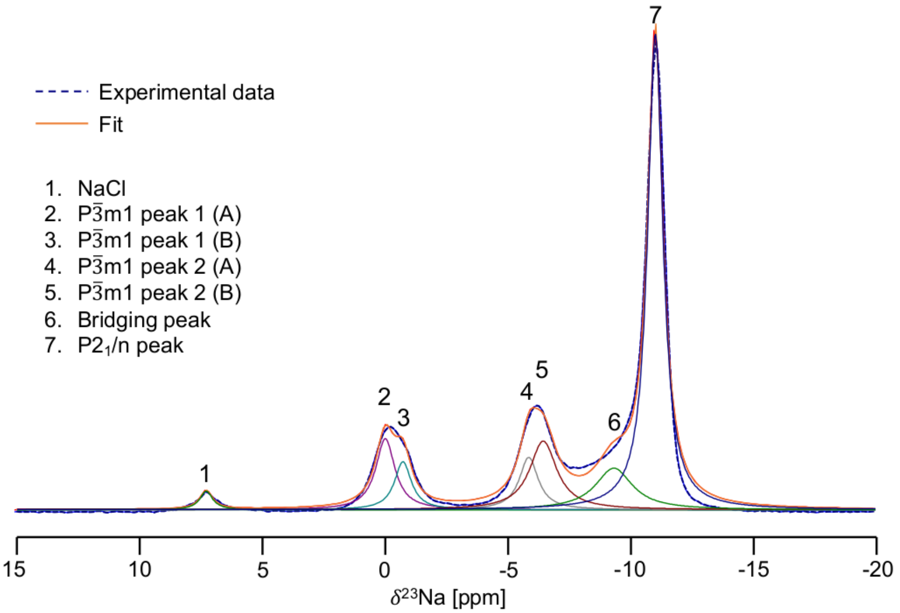

Figure S6: Example fit of a ^{23}Na MAS-NMR spectrum measured at 45 °C on twice ball milled Na_2ZrCl_6. The spectrum was acquired at 18.8 T with a 10 kHz spinning speed.

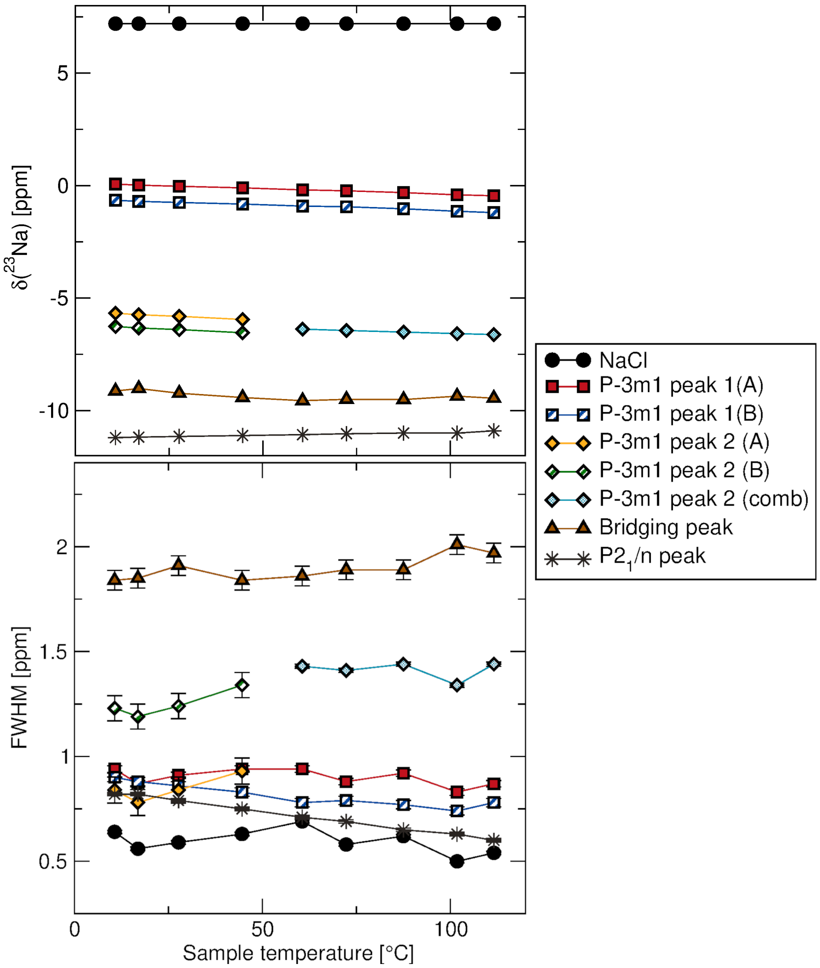

Figure S7: Evolution of the (a) isotropic shift ($\delta(^{23}$Na)) and (b) full width half max (FWHM) obtained from fits of the VT-NMR ^{23}Na MAS-NMR spectra acquired on twice ball milled Na_2ZrCl_6 between 11 and 112 °C. All lineshapes were fitted using a Lorentzian function. Above 50 °C, a single peak was required to appropriately fit the P$\bar{3}$m1 peak 2. The NaCl resonance was fixed at 7.2 ppm to serve as an internal reference. Error bars for both sets of fitting parameters (excluding the P$\bar{3}$m1 combined peak 2) were calculated from the standard deviation of values obtained from five fits of the spectrum measured at 44.6 °C, starting from different initial guesses. Error bars for the P$\bar{3}$m1 combined peak 2 were calculated at 102°C. The error bar on the fitted isotropic shifts is negligible and within the size of the labels used in this figure. Fluctuations in the FWHM values for the NaCl resonance are attributed to the small NaCl phase fraction in the sample which made the lineshape more subject to noise during each acquisition.

Sec. S7 ^{23}Na VT-NMR on Quenched Na_2ZrCl_6

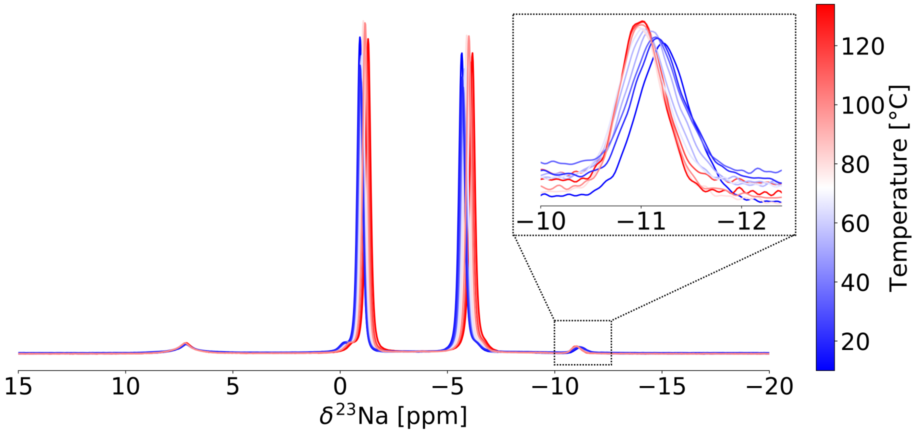

Figure S8: ^{23}**Na VT-NMR of quenched Na_2ZrCl_6 measured between 10 °C and 134 °C. Spectra are color-coded using the temperature scale on the right of the plot. The peak at 7.2 ppm corresponds to NaCl. Spectra were obtained at 18.8 T with a 10 kHz MAS spinning speed. An inset of the $P2_1/n$ resonance is provided to highlight the evolution of its isotropic shift with temperature.**

Sec. S8 XRD Patterns Obtained on Na_3YCl_6 Samples

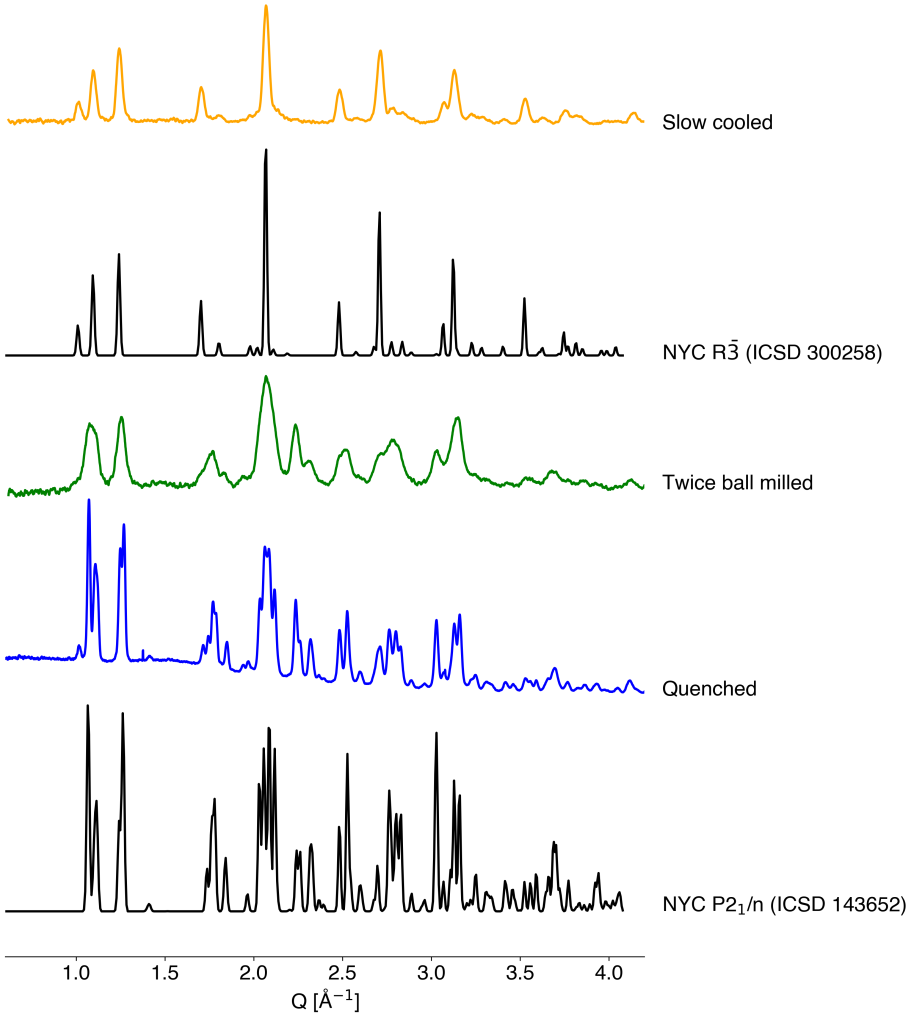

Figure S9: XRD patterns obtained on slow cooled, twice ball milled, and quenched Na_3YCl_6 along with comparisons against simulated patterns for reported structures for each Na_3YCl_6 polymorph. Patterns for the quenched and twice ball milled samples are reproduced from[1]. ICSD structures used for the simulated patterns of the $R\bar{3}$ and $P2_1/n$ Na_3YCl_6 structures are obtained from[6] and[1], respectively.

Sec. S9 SEM of Na_3YCl_6

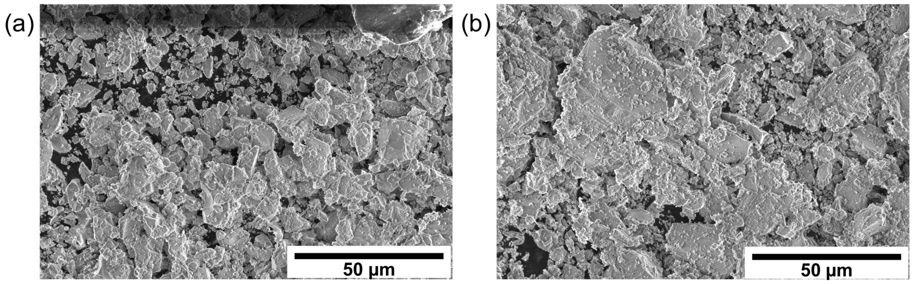

Quenched

Slow cooled

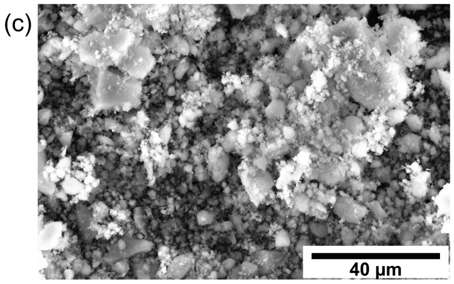

Twice ball milled

Figure S10: SEM micrographs obtained on unpressed Na_3YCl_6 powders that were prepared by initial ball milling followed by an annealing step and a (a) water bath quenching step (quenched), or (b) a 48 h slow cooling step (slow cooled). (c) After a second ball milling step of the quenched sample (twice ball milled).

Sec. S10 Simultated ^{23}Na NMR Spectrum of Na_3YCl_6

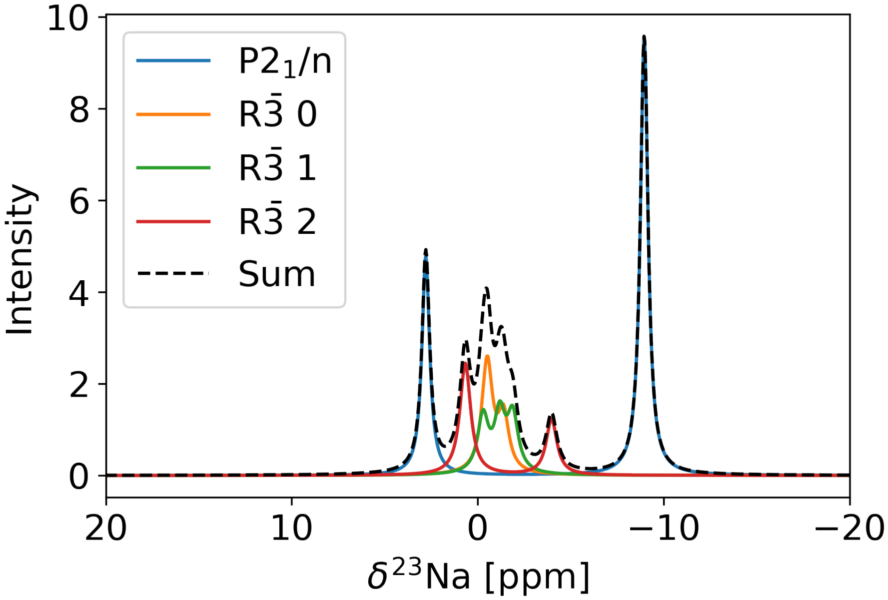

Figure S11: Reconstruction of the ^{23}Na NMR resonances expected for the Na_3YCl_6 $R\bar{3}$ and $P2_1/n$ polymorphs using Lorentzian lineshapes centered at the calibrated chemical shift values obtained from NMR CASTEP simulations and a signal linewidth of 0.7 ppm and 0.5 ppm for the $R\bar{3}$ and $P2_1/n$ forms, respectively. Various Na-vacancy orderings were enumerated for the $R\bar{3}$ structure. A larger linewidth value was used for the $R\bar{3}$ as the experimentally observed signal is expected to be an average of the shifts calculated for the various enumerated orderings due to fast Na exchange between individual sites in the $R\bar{3}$ structure on the NMR timescale.

Sec. S11 ^{23}Na EXSY on Twice Ball Milled Na_3YCl_6

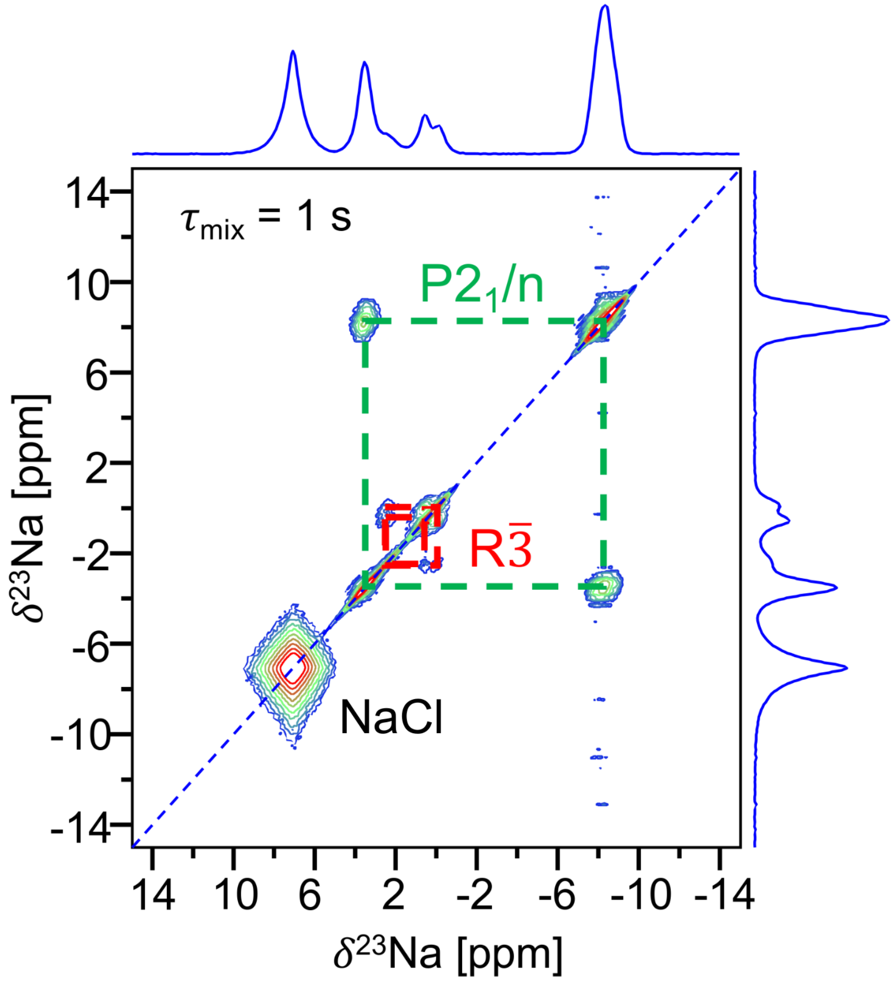

Figure S12: ^{23}Na 2D EXSY spectrum obtained on twice ball milled Na_3YCl_6 at 55 °C (328 K) and using a 1 s mixing time (τ_{mix}). The 1D spectrum collected on this sample is projected on the right hand side and at the top of the 2D spectrum. All spectra were acquired at 18.8 T using a 3.2 mm HX probe at a 10 kHz MAS spinning speed. Longitudinal relaxation times (T_1) for both Na_3YCl_6 phases were on the order of 4 s, allowing minimal signal loss during the 1 s of mixing time.

Sec. S12 ^{23}Na VT-NMR on Quenched Na_3YCl_6

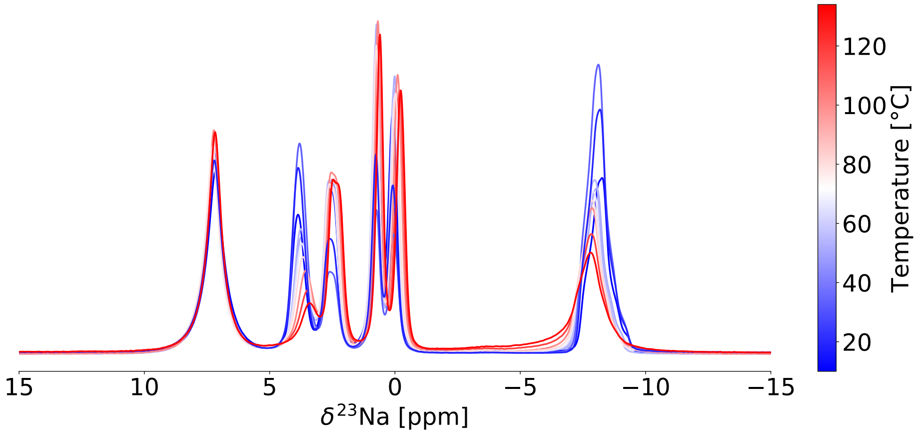

Figure S13: ^{23}Na VT-NMR on quenched Na_3YCl_6. Spectra are color-coded using the temperature scale on the right of the plot. The peak at 7.2 ppm is NaCl. All spectra were obtained at 18.8 T with a 10 kHz MAS spinning speed.

Sec. S13 Microstructure Evolution of Quenched Na_3YCl_6 upon a 134 °C Heat Treatment

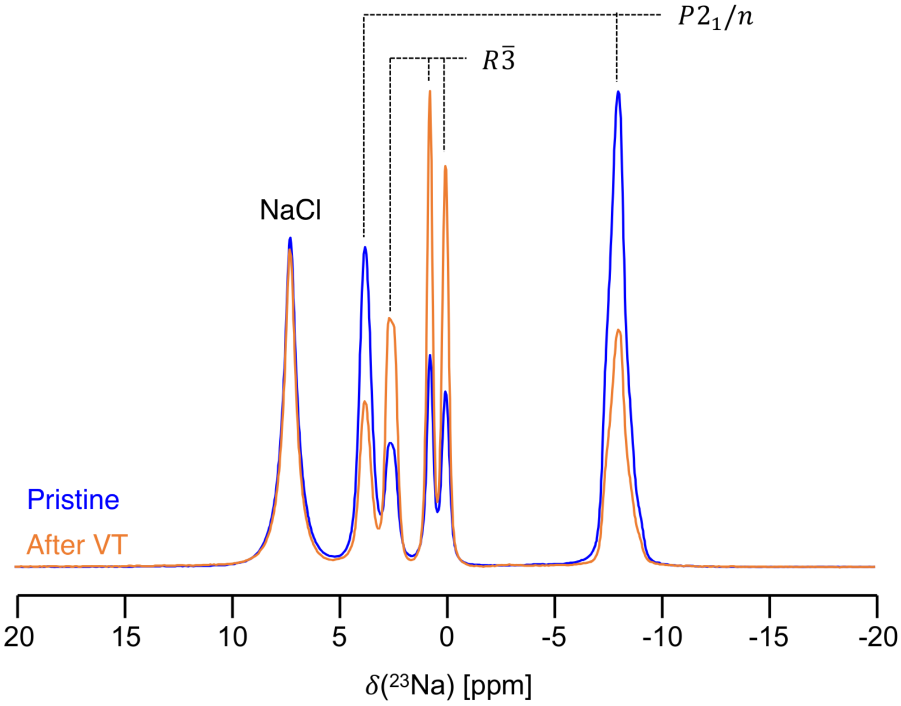

Figure S14: ^{23}Na MAS-NMR spectra collected at 52 °C (328 K) on quenched Na_3YCl_6 before and after VT-NMR measurements. Spectra were acquired at 18.8 T using a 3.2 mm HX probe at a 10 kHz MAS spinning speed. The phase fraction of the $R\bar{3}$ increases after exposure to temperatures up to 134 °C during VT-NMR measurements.

Sec. S14 Bond Valence Sum Maps of Na_2ZrCl_6 and Na_3YCl_6 Polymorphs

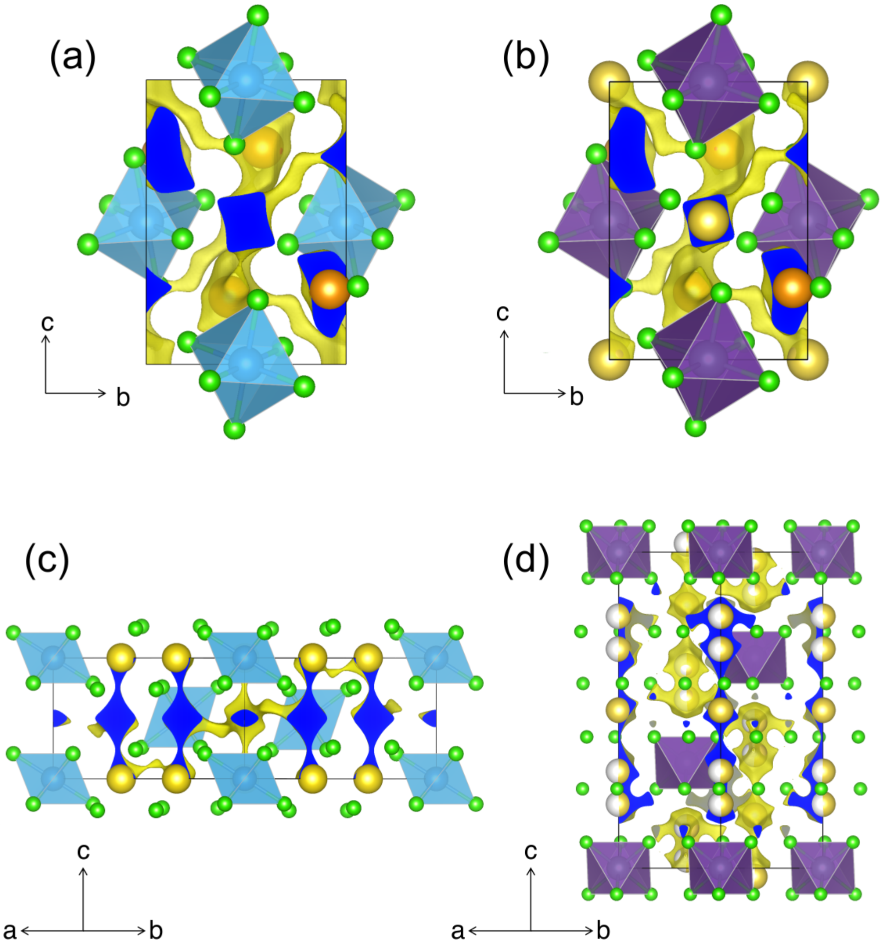

Figure S15: Bond valence sum maps calculated for the $P2_1/n$ forms of (a) Na_2ZrCl_6 and (b) Na_3YCl_6, as well as (c) $P\bar{3}m1$ Na_2ZrCl_6 and (d) $R\bar{3}$ Na_3YCl_6. Color legend: Y is purple, Zr is light blue, Cl is light green, while Na atoms in octahedral or prismatic environments are yellow and orange, respectively. Bond valence maps were calculated with softBV[7] and the visualized isosurface level was set to 0.1.

Sec. S15 Le Bail Refinement of Slow Cooled $Na_{2.25}Y_{0.25}Zr_{0.75}Cl_6$ XRD Pattern

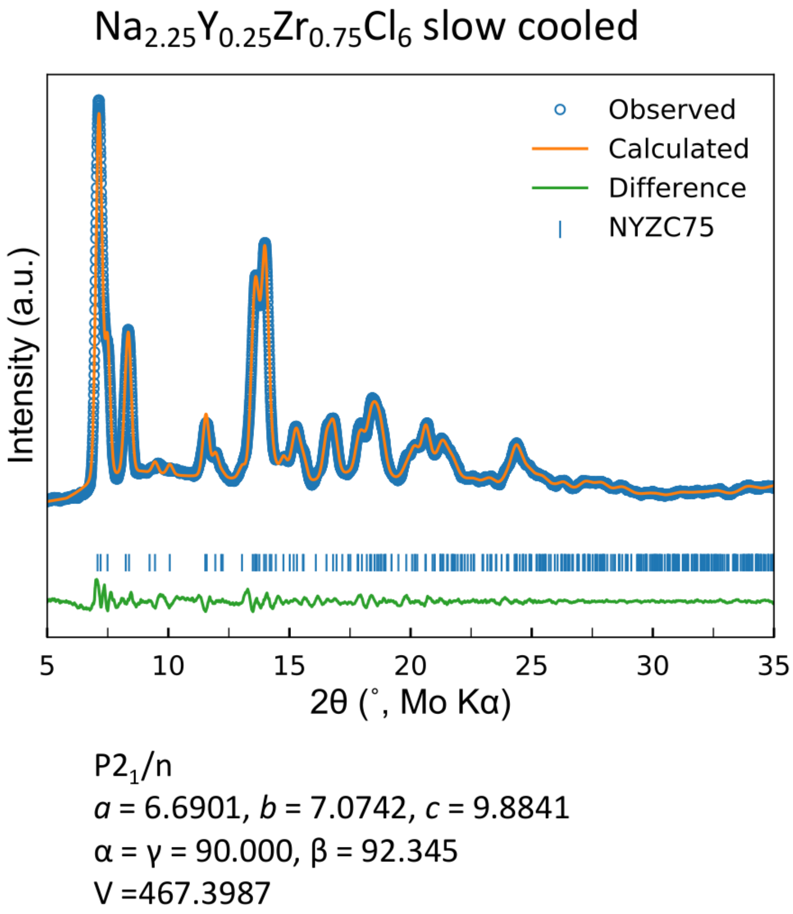

Figure S16: Le Bail refinement of the XRD pattern obtained for slow cooled $Na_{2.25}Y_{0.25}Zr_{0.75}Cl_6$.

Sec. S16 Raman of $Na_{2.25}Y_{0.25}Zr_{0.75}Cl_6$

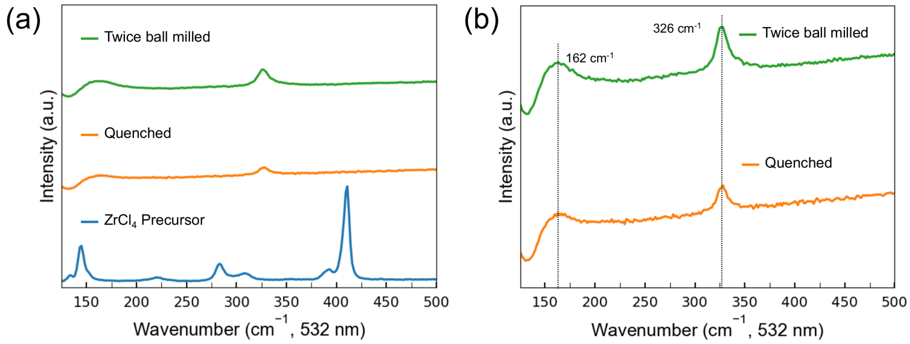

Figure S17: Raman spectra collected on twice ball milled and quenched $Na_{2.25}Y_{0.25}Zr_{0.75}Cl_6$ samples as well as a $ZrCl_4$ precursor. Spectra were obtained with a 532 nm laser source.

Sec. S17 Energetics of Enumerated $Na_{2.25}Y_{0.25}Zr_{0.75}Cl_6$ Supercells

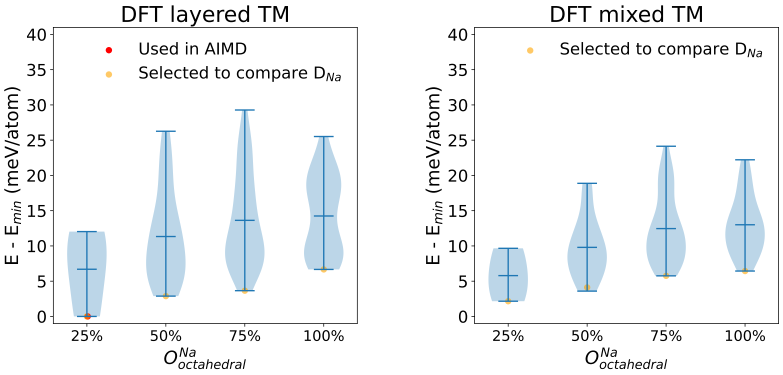

Figure S18: Energy distribution of the (a) 114 layered-TM and (b) 115 mixed-TM supercells of $Na_{2.25}Y_{0.25}Zr_{0.75}Cl_6$ simulated by DFT.

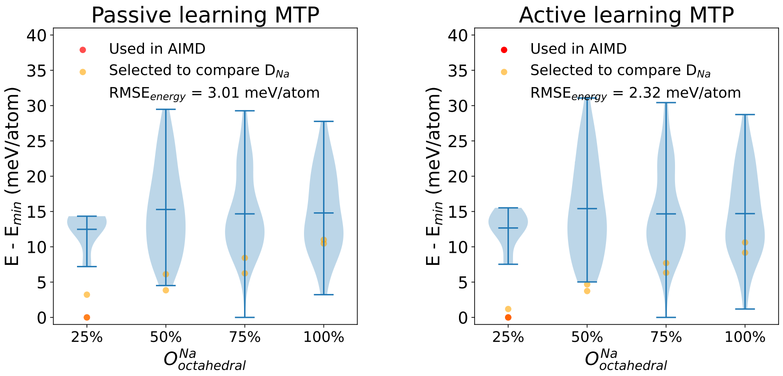

Figure S19: Energy distribution of the 229 enumerated supercells of $Na_{2.25}Y_{0.25}Zr_{0.75}Cl_6$ by (a) the passive learning MTP and (b) the active learning MTP.

Sec. S18 ^{23}Na EXSY of twice ball milled $\mathbf{Na_{2.25}Y_{0.25}Zr_{0.75}Cl_6}$

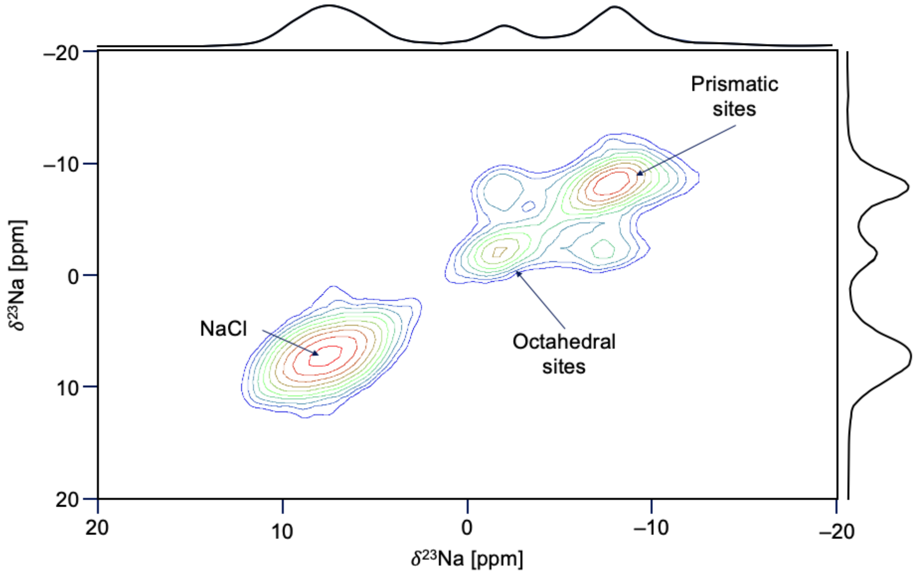

Figure S20: ^{23}Na EXSY conducted at 55 °C (328 K) on twice ball milled $\mathbf{Na_{2.25}Y_{0.25}Zr_{0.75}Cl_6}$. Spectra were acquired at 18.8 T using a 3.2 mm HX probe at a 10 kHz spinning speed with a 50 ms mixing time (τ_{mix}).

Sec. S19 Cross-sectional SEM of $Na_{2.25}Y_{0.25}Zr_{0.75}Cl_6$ Pellets

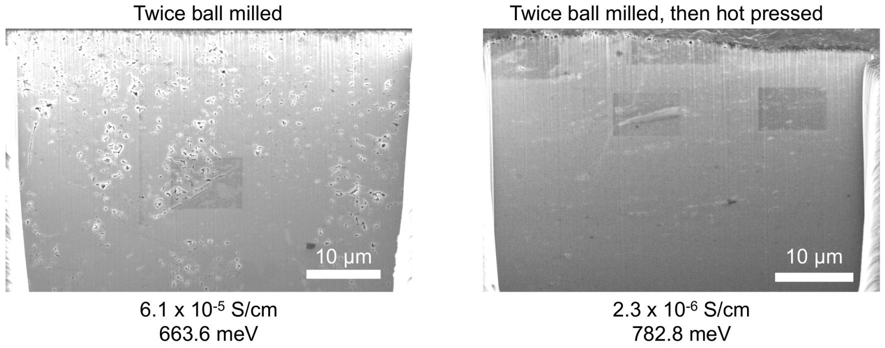

Figure S21: Cross-sectional SEM micrographs collected on (left) a twice ball milled $Na_{2.25}Y_{0.25}Zr_{0.75}Cl_6$ pellet densified under a pressure of 370 MPa at room temperature, and (right) a hot pressed, twice ball milled $Na_{2.25}Y_{0.25}Zr_{0.75}Cl_6$ pellet. Hot pressing was conducted at 300 °C at a pressure of 370 MPa for 4 hrs. Na-ion conductivities and diffusional activation energies for each sample are reported below each panel. Despite the clear decrease in the void area of the pellet upon hot pressing, Na-ion transport is severely hindered compared to the room temperature densified pellet. These findings can be accounted for by changes in the cation distribution within the bulk NYZC75 structure, as evidenced by the evolution of the ^{23}Na NMR spectra collected before and after the twice ball milled sample was exposed to 111 °C (see Figure S26). It is anticipated that such changes are even more pronounced upon hot pressing at 300 °C, leading to a more significant decrease in Na-ion conduction.

Sec. S20 Improvement of Reliability of MTP with Active Learning

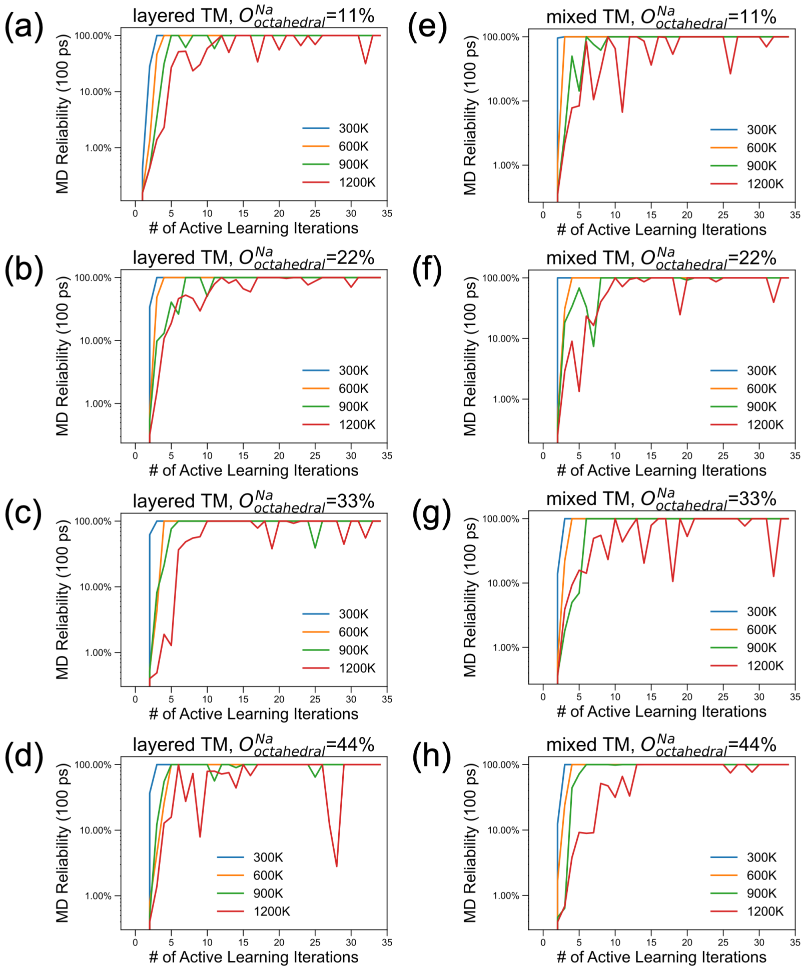

Figure S22: Improvements in the reliability of the MD simulations through active learning iterations for the MTP. Active learning iterations are performed on (a-d) four layered-TM structures and (e-h) four mixed-TM structures spanning different Na site occupancies. After 34 iterations of active learning, 100% MD reliabilities, i.e., completing 100 ps MD without any snapshot having a γ over 5 were achieved at 300 to 1200 K with 300 K intervals for all eight structures considered here.

Sec. S21 Simulated Evolution of Na Octahedral Site Occupancies in $\mathrm{Na_{2.25}Y_{0.25}Zr_{0.75}Cl_6}$

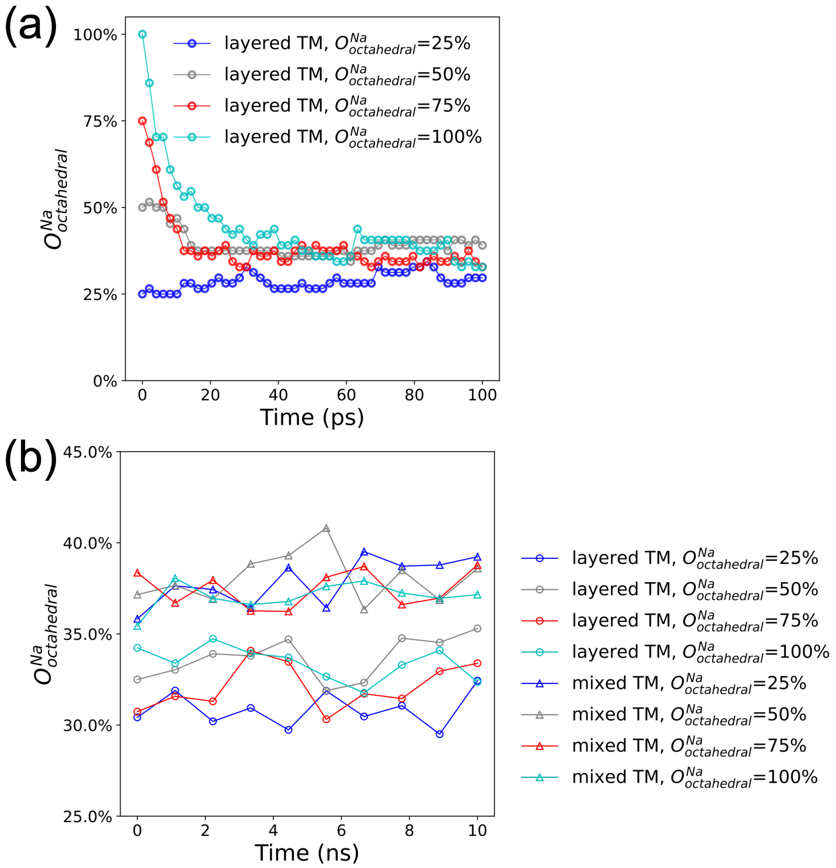

Figure S23: (a) Simulated evolution of $O^{Na}_{octahedral}$ in layered-TM structures over the first 100 ps of MD simulations conducted at 400 K. (b) The evolution of equilibrated $O^{Na}_{octahedral}$ in layered-TM and mixed-TM structures over the first 10 ns of MD simulations conducted at 400 K. Each data point was averaged over 100 trajectory snapshots.

Sec. S22 Simulated Na Motion at 500 K in $Na_{2.25}Y_{0.25}Zr_{0.75}Cl_6$

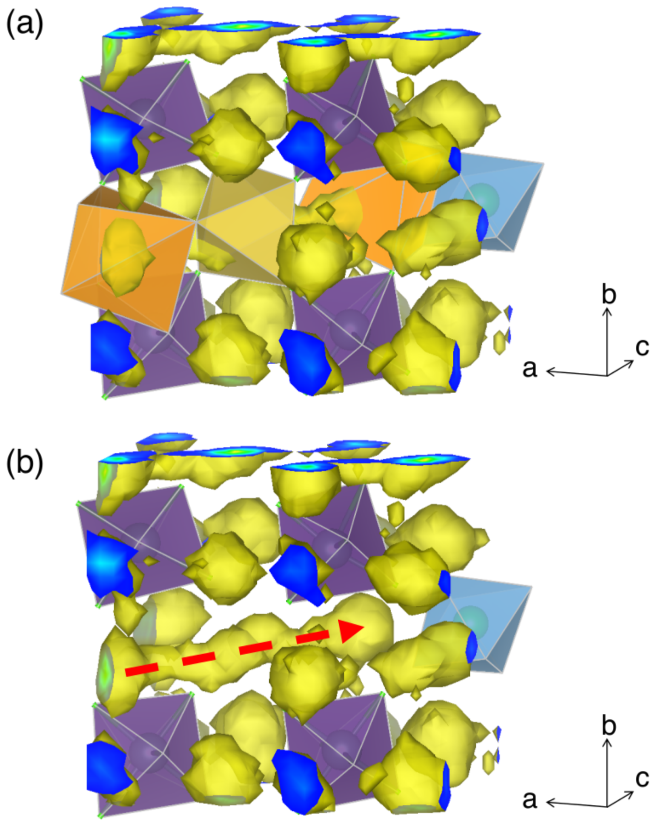

Figure S24: Plot of the Na probability density (isosurface value = 6.5×10^{-5}) in a $Na_{2.25}Y_{0.25}Zr_{0.75}Cl_6$ model supercell simulated by AIMD at 500 K in our previous work[1]. $YCl_6{}^{3-}$ and $ZrCl_6{}^{2-}$ polyhedra are shown in purple and light blue, respectively. Polyhedra for Na prismatic (orange) and octahedral (yellow) sites are displayed in panel (a), and the hopping pathway (red dashed arrow) is highlighted in panel (b). Cl atoms are omitted from the diagram for clarity.

Sec. S23 Simulated Cl Motion at 400 K in $Na_{2.25}Y_{0.25}Zr_{0.75}Cl_6$

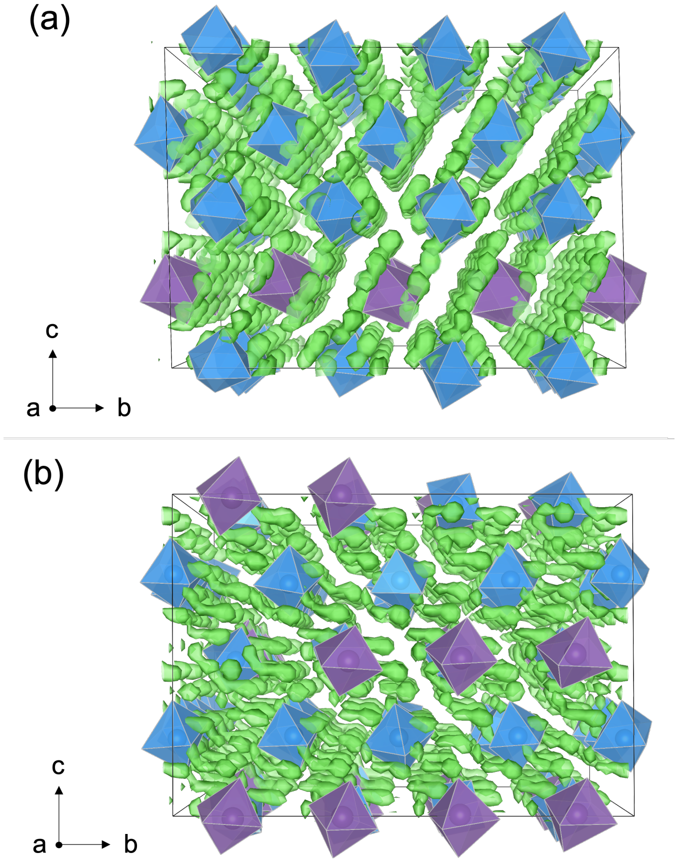

Figure S25: Plots of the Cl probability density (isosurface value = 3×10^{-4}) of Cl^- in (a) layered-TM and (b) mixed-TM structures of $Na_{2.25}Y_{0.25}Zr_{0.75}Cl_6$ simulated by MTP at 400 K. Color legend: Y is purple, Zr is light blue, and Cl is light green. Na is not displayed for visual clarity.

Sec. S24 Evolution of Twice Ball Milled $Na_{2.25}Y_{0.25}Zr_{0.75}Cl_6$ EIS-derived Conductivity

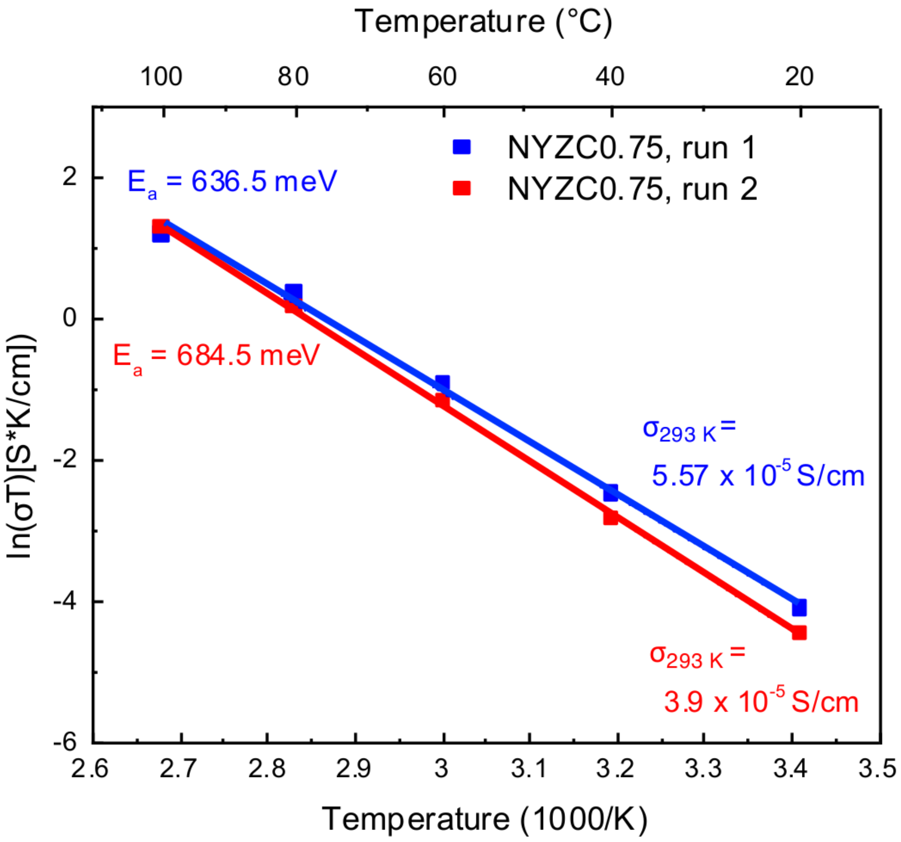

Figure S26: Successive temperature ramp EIS measurements on twice ball milled $Na_{2.25}Y_{0.25}Zr_{0.75}Cl_6$. Impedance spectra were obtained at regular 20 °C increments as the temperature of the sample was increased from 20 °C to 100 °C. The sample temperature was then decreased back down to 20 °C and the process was repeated to assess the impact of heating on the sample conductivity.

Sec. S25 Metastability of the Twice Ball Milled $Na_{2.25}Y_{0.25}Zr_{0.75}Cl_6$ Structure

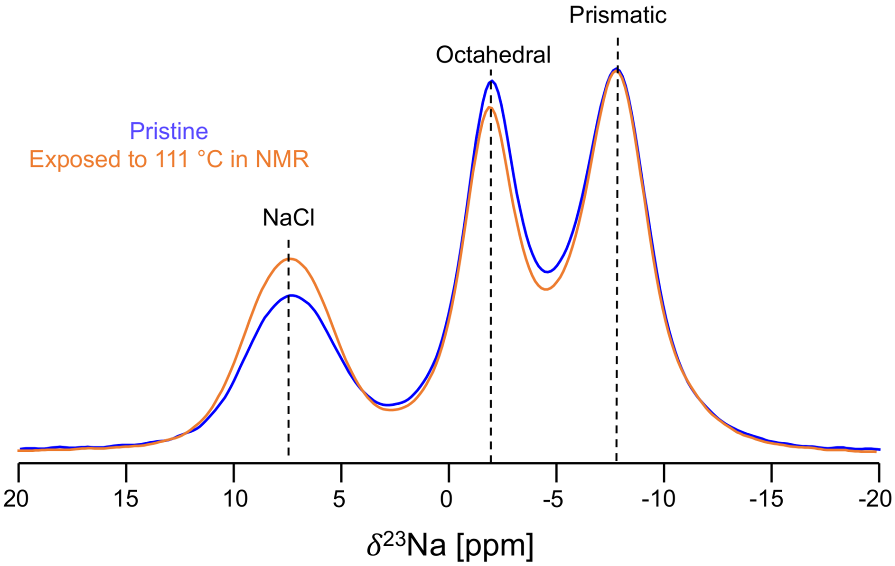

Figure S27: ^{23}**Na MAS-NMR obtained at 55 °C on a twice ball milled $Na_{2.25}Y_{0.25}Zr_{0.75}Cl_6$ sample in its pristine state and after overnight exposure to temperatures up 111 °C. Spectra were acquired at 18.8 T with a 12 kHz spinning speed. Octahedral site occupancy decreases while the NaCl impurity over the course of the high temperature exposure.**

Sec. S26 Building NYC, NZC, and NYZC structural models for NMR CASTEP calculations

The strategies used to build NYC, NZC, and NYZC structural models for NMR CASTEP calculations are described below:

Sec. S26.1 NZC

The $P\bar{3}m1$ structure was based on the model generated in our previous work[1]. Four structures were enumerated with differing Na occupations (i.e. Na split between the $6g$ and $6h$ sites) and Zr occupation of the $1a$ and z=0 and z=0.5 $2d$ Wyckoff sites, emulating the M1-M2-M3 disorder described in Li_3YCl_6 by Schlem *et al.*[8]. NMR CASTEP calculations were run on these enumerated structures.

The $P2_1/n$ structure was taken from a experimentally observed Na_2IrCl_6 structure[9], with Ir replaced by Zr. The structure was then relaxed with CASTEP and its NMR shift was computed.

Sec. S26.2 NYC

The $R\bar{3}$ structural model was based on the reported refined structure from Stenzel *et al.*[6] with partial Na occupation across the 6c sites and complete occupation of the 3c site. Structures were enumerated from this model and relaxed using CASTEP. Finally, isotropic shifts were computed on each of these structures.

The $P2_1/n$ structural model was based on the model generated by Rietveld refinements in our previous work[1]. The structure was relaxed and its shifts were calculated using CASTEP.

Sec. S26.3 NYZC

A structural model with partial Na occupation of the octahedral and prismatic sites as well as split Y-Zr occupation of the transition metal sites was taken from our previous work[1]. Structures with differing Na-vacancy and Y-Zr distributions were enumerated from this model. Of the enumerated structures, 11 symmetrically inequivalent structures that were within 10 meV/atom of the lowest energy structure were used for calculations. ^{23}Na isotropic shift values were then correlated with their local environments to gain intuition on the effect of site coordination (i.e. octahedral vs prismatic) as well as neighboring transition metal species (number of neighboring ${ZrCl_6}^{2-}$ and ${YCl_6}^{3-}$ octahedra).

Sec. S27 Parameter Convergence for NMR CASTEP Calculations

Table S1: NMR CASTEP calculations parameters. For geometry optimization calculations, plane wave energy cutoffs (in Ry) and *k*-point grids were selected based on a 0.5 meV atom^{-1} convergence criterion for single point energy calculations. An isotropic chemical shielding constant convergence criterion of 0.5 ppm was used for ^{23}Na NMR parameters. For consistency, all NMR parameter calculations used an 80 Ry plane wave energy cutoff.

	Geometry optimization		**NMR calculations**	
Compound	***k*-point grid**	**cutoff**	***k*-point grid**	**cutoff**
NaCl	4×4×4	50	4×4×4	80
Na_2O	4×4×4	80	4×4×4	80
Na_2S	4×4×4	60	4×4×4	80
Na_2S_2	6×6×3	70	8×8×4	80
NaBr	4×4×4	60	4×4×4	80
NaF	4×4×4	70	4×4×4	80
NaOH	6×2×6	70	6×2×6	80
Na_2ZrCl_6, $P\bar{3}m1$	3×3×6	50	3×3×6	80
Na_2ZrCl_6, $P2_1/n$	3×3×2	50	6×6×4	80
Na_3YCl_6, $P2_1/n$	3×3×2	60	4×4×3	80
Na_3YCl_6, $R\bar{3}$	3×3×3	60	3×3×3	80
$Na_{2.25}Y_{0.25}Zr_{0.75}Cl_6$ (1)	3×3×1	50	4×4×2	80
$Na_{2.25}Y_{0.25}Zr_{0.75}Cl_6$ (2)	3×3×2	50	4×4×3	80

Sec. S28 ^{23}Na Chemical Shift Calibration Curve for Analysis of NMR CASTEP Calculation Results

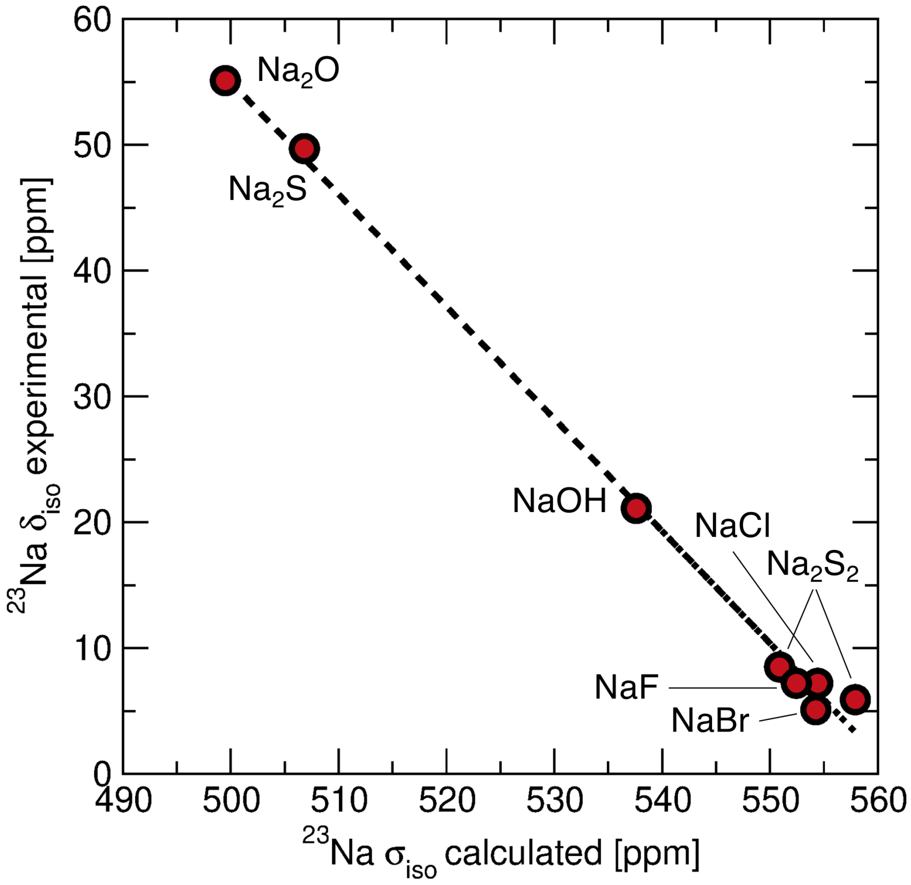

Figure S28: ^{23}Na NMR semi-empirical calibration curve for converting CASTEP-calculated σ_{iso} values to experimentally-relevant δ_{iso} values.

Table S2: NMR CASTEP-calculated σ_{iso} and experimentally measured δ_{iso} for compounds selected for ^{23}Na NMR calibration curve. δ_{iso} is referenced to 1 M NaCl (aq.).

Compound	**CASTEP σ_{iso}**	δ_{iso}	**Reference**
NaCl	554.43	7.2	10
Na_2O	499.49	55.1	11
Na_2S	506.83	49.7	12
Na_2S_2	550.88	8.5	12
Na_2S_2	557.91	5.9	12
NaBr	554.25	5.1	10
NaF	552.44	7.2	10
NaOH	537.6	21.1	10

References

[1] E. A. Wu, S. Banerjee, H. Tang, P. M. Richardson, J.-M. Doux, J. Qi, Z. Zhu, A. Grenier, Y. Li, E. Zhao, G. Deysher, E. Sebti, H. Nguyen, R. Stephens, G. Verbist, K. W. Chapman, R. J. Clément, A. Banerjee, Y. S. Meng and S. P. Ong, *Nat Commun*, 2021, **12**, 1256.

[2] E. Sebti, H. A. Evans, H. Chen, P. M. Richardson, K. M. White, R. Giovine, K. P. Koirala, Y. Xu, E. Gonzalez-Correa, C. Wang, C. M. Brown, A. K. Cheetham, P. Canepa and R. J. Clément, *J. Am. Chem. Soc.*, 2022, **144**, 5795–5811.

[3] M. A. Plass, S. Bette, R. E. Dinnebier and B. V. Lotsch, *Chem. Mater.*, 2022, **34**, 322–3235.

[4] Z. Liu, S. Ma, J. Liu, S. Xiong, Y. Ma and H. Chen, *ACS Energy Lett.*, 2020, **6**, 298–304.

[5] M. Casas-Cabanas, M. Reynaud, J. Rikarte, P. Horbach and J. Rodríguez-Carvajal, *J Appl Crystallogr*, 2016, **49**, 2259–2269.

[6] F. Stenzel and G. Meyer, *Z. Anorg. Allg. Chem.*, 1993, **619**, 652–660.

[7] H. Chen, L. L. Wong and S. Adams, *Acta Cryst B*, 2019, **75**, 18–33.

[8] R. Schlem, S. Muy, N. Prinz, A. Banik, Y. Shao-Horn, M. Zobel and W. G. Zeier, *Adv. Energy Mater.*, 2019, **10**, 1903719.

[9] S.-S. Bao, D. Wang, X.-D. Huang, M. Etter, Z.-S. Cai, X. Wan, R. E. Dinnebier and L.-M. Zheng, *Inorg. Chem.*, 2018, **57**, 13252–13258.

[10] S. F. Dec, G. E. Maciel and J. J. Fitzgerald, *J. Am. Chem. Soc.*, 1990, **112**, 9069–9077.

[11] G. Klösters and M. Jansen, *Solid State Nuclear Magnetic Resonance*, 2000, **16**, 279–283.

[12] G. Mali, M. U. M. Patel, M. Mazaj and R. Dominko, *Chem. Eur. J.*, 2016, **22**, 3355–3360.